Cell Reports
Physical Science

CellPress
OPEN ACCESS

Article

Chemical Microrobots as Self-Propelled Microbrushes against Dental Biofilm

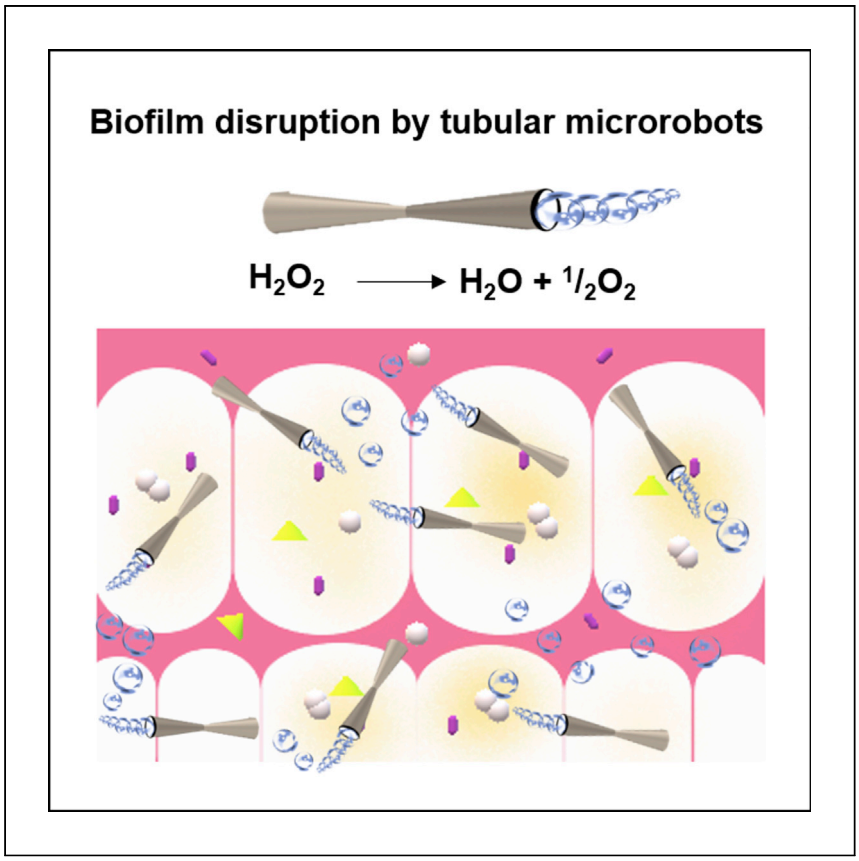

Autonomous self-propelled tubular microrobots based on titanium dioxide decorated with platinum nanoparticles were developed by Villa et al. for the degradation of dental biofilm strains. The killing ability of these micromachines is attributed to their antibacterial activity and the continuous generation of microbubbles at the biofilm surface.

Katherine Villa, Jitka Viktorova, Jan Plutnar, Tomáš Ruml, Lan Hoang, Martin Pumera

pumera.research@gmail.com

HIGHLIGHTS

The ability of catalytic microrobots to disrupt dental biofilm is demonstrated

95% killing efficiency is obtained after 5 min of treatment

The biocompatibility of these microrobots with epidermal and organ cells is confirmed

Villa et al., Cell Reports Physical Science *1*, 100181
September 23, 2020
https://doi.org/10.1016/j.xcrp.2020.100181

Cell Reports
Physical Science

CellPress
OPEN ACCESS

Article

Chemical Microrobots as Self-Propelled Microbrushes against Dental Biofilm

Katherine Villa,[1] Jitka Viktorova,[2] Jan Plutnar,[1] Tomáš Ruml,[2] Lan Hoang,[2] and Martin Pumera[1,3,4,5,6,*]

SUMMARY

Mouths offer the perfect environments for microbial cell formation, promoting the growth of biofilms, for example, on teeth. Dental biofilm exhibits strong resistance to antibiotics and is a cause of many dental diseases. Common strategies for dental biofilm removal involve the addition of high concentrations of hydrogen peroxide (H_2O_2), which increases tooth sensitivity, or mechanical procedures. Here, we report a different approach based on self-propelled micromachines with high antibacterial activity for the degradation of dental biofilm. Such microrobots use low concentrations of fuel for their propulsion, and they achieve an efficient dental biofilm disruption in only 5 min of treatment. Moreover, these microrobots are biocompatible with epidermal and organ cells and may stimulate the immune system to fight against microbial infection. This approach of exploiting the active motion of bubble-propelled catalytic micromachines for oral biofilm disruption may open the door for more efficient and sophisticated treatments in dentistry.

INTRODUCTION

Microrobots/nanorobots (also called micromotors/nanomotors) have attracted considerable attention over the last decade because of their unique capabilities of self-propulsion in diverse liquid environments to target specific tasks at the microscale/nanoscale.[1] In particular, these devices have demonstrated important advances in the biomedical field.[2,3] For instance, their active motion has resulted in more efficient drug-delivery treatments compared to passive particles. These devices have also been successfully used in cell manipulation,[4] cargo transportation,[5,6] and biosensing.[7,8]

Over the years, different types of microrobots/nanorobots that can move either in the presence of chemical fuels or under the application of external fields have been developed.[9] Among them, catalytic machines composed of a catalytic engine (Pt) that enables the catalytic decomposition of hydrogen peroxide (H_2O_2) into oxygen (O_2) molecules remain the most studied type.[1] Depending on their size, the motion mechanism can be classified as self-diffusiophoresis or bubble propulsion.[10,11] The latter usually exhibits strong bubble thrust and higher speeds.[12] However, their application in the biomedical field is limited due to the well-known toxicity of H_2O_2.

Dental biofilm, also known as dental plaque, is a causative agent of dental diseases, such as caries, gingivitis, and periodontitis.[13] Dental biofilm is mostly composed of diverse types of bacteria that stick to one another on the surface of teeth or dental implants.[14] Since the whole biofilm is protected by a self-produced matrix of organic polymers, this type of microbial infection is more resistant to therapeutic procedures and immune system responses in comparison to planktonic (free) bacteria.[15]

[1]Center for Advanced Functional Nanorobots, Department of Inorganic Chemistry, University of Chemistry and Technology Prague, Technická 5, 166 28 Prague, Czech Republic

[2]Department of Biochemistry and Microbiology, University of Chemistry and Technology Prague, Technická 5, 166 28 Prague, Czech Republic

[3]Future Energy and Innovation Laboratory, Central European Institute of Technology, Brno University of Technology, Purkyňova 656/123, 616 00 Brno, Czech Republic

[4]Department of Chemical and Biomolecular Engineering, Yonsei University, 50 Yonsei-ro, Seodaemun-gu, Seoul 03722, Korea

[5]Department of Medical Research, China Medical University Hospital, China Medical University, No. 91 Hsueh-Shih Road, Taichung, Taiwan

[6]Lead Contact

*Correspondence: pumera.research@gmail.com

https://doi.org/10.1016/j.xcrp.2020.100181

Likewise, the efficacy of the applied mechanical or chemical treatment is rather restricted due to the poor reachability to interdental cavities.[16] Therefore, an exploration of alternative treatments that exhibit efficient antibiofilm activity is required.

Here, we present self-propelled tubular microrobots that are able to efficiently disrupt a synthetic biofilm composed of a mixture of dental strains by the combination of an autonomous generation of microbubbles with the *in situ* formation of reactive species, such as hydroxyl radicals, on the biofilm surface. These devices consist of a biocompatible material (titanium dioxide, TiO_2) decorated with Pt nanoparticles (NPs) in the inner surface, which are responsible for fuel decomposition. Since H_2O_2 is a safe oxidant agent for dental disinfection procedures, the combination of the autonomous movement of these antibacterial microrobots in such treatments results in a synergistic effect that boosts biofilm degradation rates. Because of their tiny sizes and autonomous motion, these micromachines hold the potential for wider reachability of dental cavities, which is difficult to achieve by the current approaches. Overall, this work represents an innovative application of catalytic microrobots in dental procedures.

RESULTS AND DISCUSSION

Synthesis and Characterization of Microrobots

Considering that tubular micromachines have demonstrated more efficient bubble propulsion than spherical ones,[17] we opted for the development of tubular TiO_2/Pt microrobots. Previous works have documented the fabrication of single-component TiO_2 tubular micromotors by dry spinning[18] or rolled-up technologies.[19] However, the resulting tubular structures consist of heterogeneous sizes with limitations regarding the size variability. In this work, we present the synthesis of biconical TiO_2-based microrobots by a combination of atomic layer deposition (ALD) and commercial membranes, without requiring a silica matrix.[20]

Figure 1 is a schematic illustration of the fabrication process and characterization of the TiO_2/Pt microrobots. The tubular morphology was obtained by using a biconical membrane of 2 μm pore diameter as a template. TiO_2 was grown inside the membrane using ALD. Afterward, the Pt NPs were photodeposited inside the tubes under UV-visible light irradiation in the presence of ethanol as a sacrificial agent. Then, the TiO_2/Pt tubes were released by dissolving the membrane in dichloromethane (Figure 1A). The characterization of the TiO_2/Pt microrobots was performed by scanning electron microscopy (SEM), scanning transmission electron microscopy (STEM), Fourier transform infrared spectroscopy (FTIR), and X-ray diffraction (XRD). Figure 1B shows the SEM image of the TiO_2/Pt microrobots, which consist of a biconical tubular morphology. Such an asymmetrical tubular structure is advantageous for efficient bubble propulsion.[21] The tubes exhibit an average maximum length of 17 $\pm$ 2 μm and a diameter of 2 $\pm$ 0.2 μm (estimated from the SEM images of 40 tubes). As is evident by the SEM magnification image shown in Figure 1C, the thickness of the TiO_2 layer was found to be ~200 nm. The STEM image confirms the hollow tubular structure of the microrobots. Moreover, it shows the homogeneity of the tubes in terms of shape and length (Figure 1D). Tiny nanotubes with a diameter of up to 100 nm can also be obtained by changing the membrane pore size from 2 μm to 100 nm, which shows the versatility and shape reproducibility that this methodology offers for the fabrication of nano- and microrobots (see Figure S1). The energy-dispersive X-ray (EDX) mapping images confirm the presence of Ti, O, and Pt in the structure of the microrobots (Figures 1E–1G), showing that the Pt NPs are mostly accumulated at the edges of the tubes (Figure 1G). Furthermore, the EDX spectrum corroborates the presence of Ti, O, and Pt. Likewise, some C and Cl element impurities are also seen, due to the release/washing of the tubes with the organic solvent (see Figure S2). The FTIR

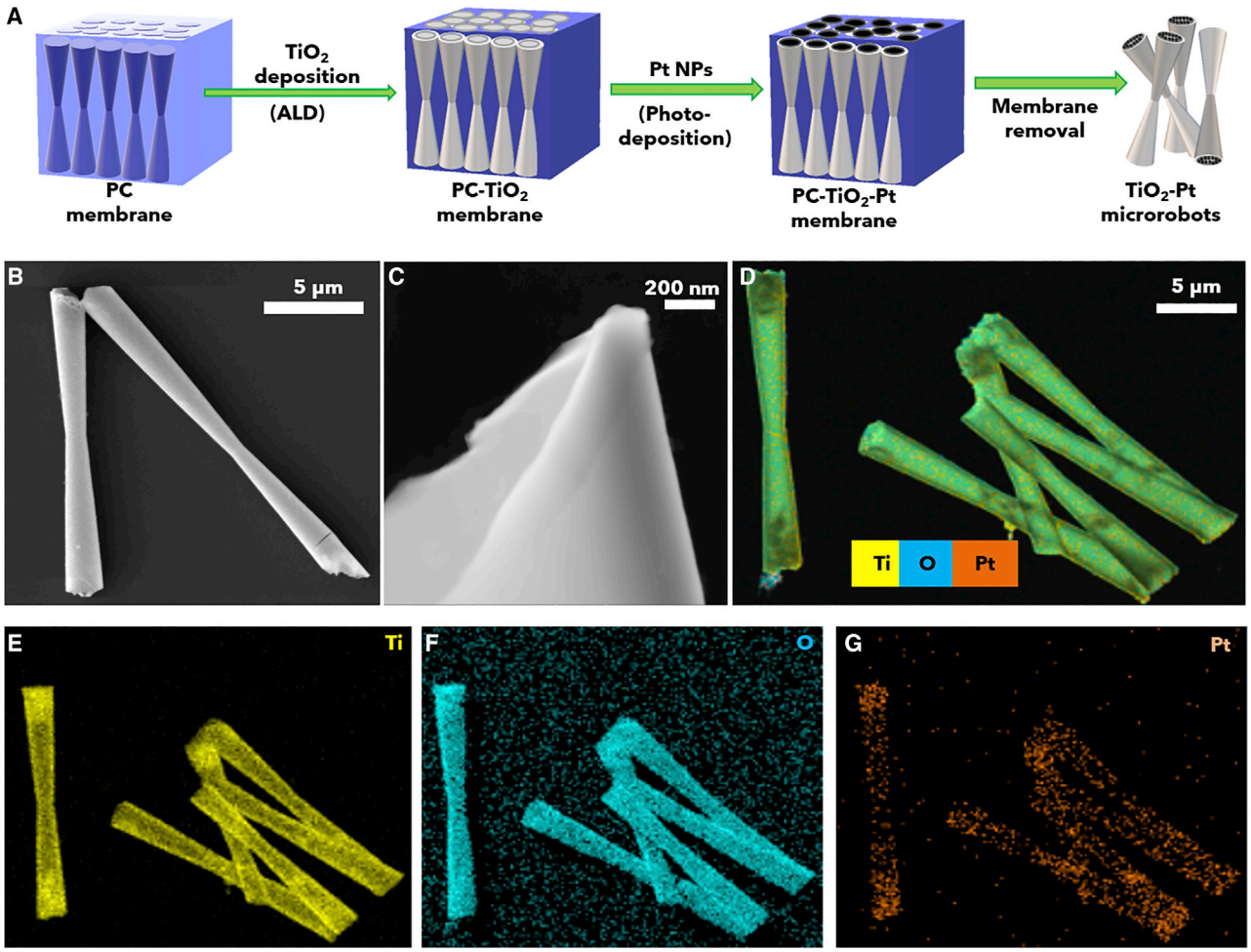

Figure 1. Fabrication and Characterization of TiO_2/Pt Tubular Microrobots

(A) Schematic illustration of the synthesis of TiO_2/Pt microrobots by ALD and photodeposition methods.

(B) SEM image of TiO_2/Pt microrobots.

(C) Magnification of an SEM image showing the thickness of TiO_2 tubes.

(D) STEM image of TiO_2/Pt microrobots.

(E–G) EDX mapping images of TiO_2/Pt microrobots.

spectrum of TiO_2/Pt microrobots is shown in Figure S3. A wide peak centered at 3,350 cm^{-1} that corresponds to the stretching vibration of –OH groups from the Ti–OH bonding and/or water adsorbed on the microrobots is observed. Two small bands at 1,131 and 1,052 cm^{-1} corresponding to the symmetric and asymmetric modes of the Ti–O–C bond are also identified.[22] Such bands may be attributed to the residual C from the polycarbonate template. The characteristic peak of the Ti–O vibration at ~528 cm^{-1} from the TiO_2 structure is also detected.[23] Since the TiO_2 ALD-deposition temperature is limited by the polycarbonate membrane resistance, the fabrication procedure was performed at 120°C. As a result, the TiO_2/Pt microrobots exhibit a non-crystalline structure (see Figure S4).

The motion mechanism of the microrobots is mediated by the catalytic decomposition of H_2O_2 into H_2O and O_2 by the Pt NPs present in the inner surface. This leads to the formation, nucleation, and expulsion of O_2 bubbles from one end of the tube that triggers its motion in the opposite direction. Figure 2A shows a representative

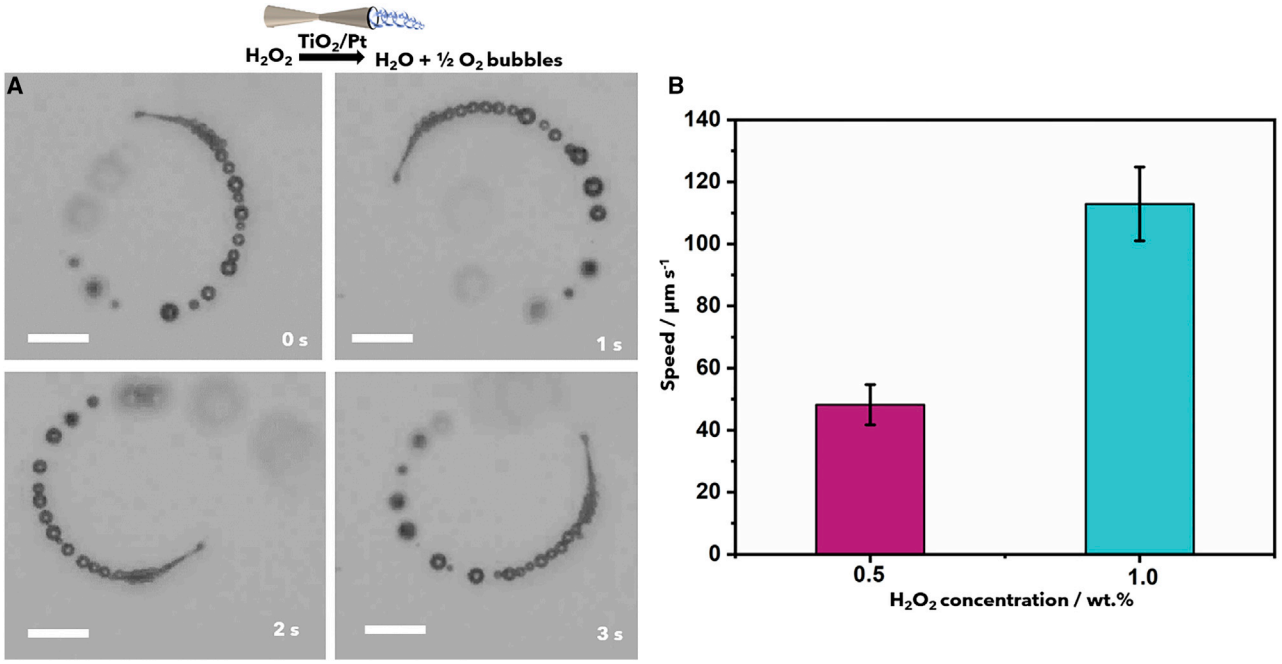

Figure 2. Motion Characterization of TiO_2/Pt Microrobots

(A) Snapshot images of TiO_2/Pt microrobots moving in a solution of 0.5 wt% H_2O_2 and 0.1 wt% surfactant. Scale bars: 10 μm.

(B) Speed of the TiO_2/Pt microrobots at different concentrations of H_2O_2 (n = 10; error bars represent the standard deviation).

motion style of the TiO_2/Pt microrobots by bubble propulsion mechanism in the presence of H_2O_2 (see Video S1). As can be seen from the tracking trajectories included in Figure S5, these microrobots mainly move by following circular trajectories, due to the asymmetrical distribution of the Pt NPs inside the microrobots.[24] However, straight swimming trajectories were also observed (see Video S2).

At low H_2O_2 concentrations, the TiO_2/Pt microrobots were able to move for a period of up to 10 min. However, their motion can be easily re-established by adding more fuel to the solution. Keeping in mind that high concentrations of H_2O_2 may involve secondary effects in dental treatments,[25,26] we examined only the motion capabilities of our micromotors at a minimum fuel concentration of 0.5 and 1 wt%. Figure 2B shows the speed of the microrobots at these fuel concentrations. Unlike other tubular microrobots that were based on photocatalytic materials of similar sizes,[27,28] these TiO_2/Pt micromachines were able to efficiently swim at 0.5 and 1 wt% fuel concentration by exhibiting maximum speeds of 48 $\pm$ 6 and 113 $\pm$ 12 μm s^{-1}, respectively. These values are comparable with other speeds shown by bubble-propelled microrobots synthesized by electrochemical methods.[29,30]

Disruption of Dental Biofilm Strains

Previous works have studied the application of microrobots in targeting different types of biofilms. For instance, Stanton et al.[31] reported biohybrids based on magnetotactic bacteria for *Escherichia coli* antibiofilm activity under magnetic fields. Likewise, a recent study demonstrated the potential of catalytic microrobots composed of Fe_3O_4 NPs for the degradation and removal of a *Streptococcus mutans* biofilm on biotic and abiotic surfaces under external magnetic actuation.[32] Inspired by these pioneering works, the main purpose of the present article was to exploit the antibacterial performance of bubble-propelled TiO_2/Pt microrobots in the

disruption of dental biofilm strains as a novel approach that does not involve the application of external magnetic fields.

Conventional procedures for treating dental biofilm plaque include the use of antiseptic agents such as chlorhexidine (CHX) and H_2O_2.[33] Some studies have shown that CHX has a limited effect on biofilm degradation and has some undesirable effects, such as tooth staining.[33–35] Since our microrobots require the addition of H_2O_2 for their propulsion, we only studied the synergistic interaction between H_2O_2 and the autonomous self-propelled TiO_2/Pt microrobots. For this purpose, we selected a dental biofilm model consisting of a mixture of dental strains, including *S. gordonii*, *Veillonella parvula*, *Fusobacterium nucleatum subsp. Nucleatum*, and *Actinomyces naeslundi*.

Initially, we performed a screening on the effect of different H_2O_2 concentrations on the viability of the dental biofilm. As shown in Figure 3A, it was found that at up to 1 wt% concentration, H_2O_2 was not toxic for the *in vitro* biofilm model system. According to the US Food and Drug Administration's (FDA's) and the International Organization for Standardization's (ISO's) standards, only viability values <80% are considered cytotoxic.[36] Therefore, we selected 1 wt% H_2O_2 as the optimal concentration for the dental biofilm viability tests. It should be noted that higher H_2O_2 concentrations (~6 wt%) are usually considered a safe dose for the limited treatment of gingival infections or teeth whitening. Such discrepancies with our findings may be attributed to the complexity of the oral cavity, which contains diverse enzymes that are able to react with H_2O_2, leading to different chemical sensitivities.[37]

Figure 3B shows the viability of the dental biofilm after treatment with different concentrations of the TiO_2/Pt microrobots and their combination with 1 wt% H_2O_2. Considering that H_2O_2 can harm oral soft and hard tissues when applied in high concentrations at long exposure times,[25,26] the multispecies dental biofilm was treated for only 5 min. Video S3 shows the autonomous motion of TiO_2/Pt swimming in H_2O_2 from 1 to 5 min. The viability of the biofilm was estimated by the resazurin-based staining method by following the pink fluorescent resorufin product. The intensity of the generated fluorescence is proportional to the metabolically active cells present in the biofilm.[38] We were surprised to find that, even in the absence of H_2O_2, the TiO_2/Pt microrobots themselves have strong antibacterial activity against the tested biofilm model. Their toxicity increased by increasing the number of microrobots. However, the combination of TiO_2/Pt microrobots with 1 wt% H_2O_2 leads to the highest biofilm removal (killing effect of up to 95%). The addition of the fuel leads to a statistically significant improvement in biofilm removal (see Table S1). From a cost-effective point of view, the fact that lower concentration of microrobots in combination with H_2O_2 achieve such efficient removal rates is very promising for future real-world applications.

Commonly, the antibacterial activity of TiO_2 under UV light has been attributed to the generation of reactive oxygen species (ROS) upon illumination, which causes oxidative cell death. However, several publications have appeared in recent years documenting that TiO_2 is able to generate reactive radicals (e.g., hydroxyl radicals), even under dark conditions.[39–42] Such radical generation without light irradiation has been observed for amorphous, anatase, and rutile TiO_2 phases,[43] and it is mainly mediated by the reaction between the TiO_2 surface and dissolved O_2.[44] Moreover, the generation of the ROS by TiO_2 may be enhanced by the addition of H_2O_2 through a Fenton-like mechanism, enhancing the oxidizing effect of TiO_2 in the dark.[40,41,45] In addition to these properties of TiO_2, the TiO_2/Pt microrobots are able to simultaneously decompose the H_2O_2 into O_2 bubbles. Therefore, the overall killing effect of the TiO_2/Pt microrobots may be

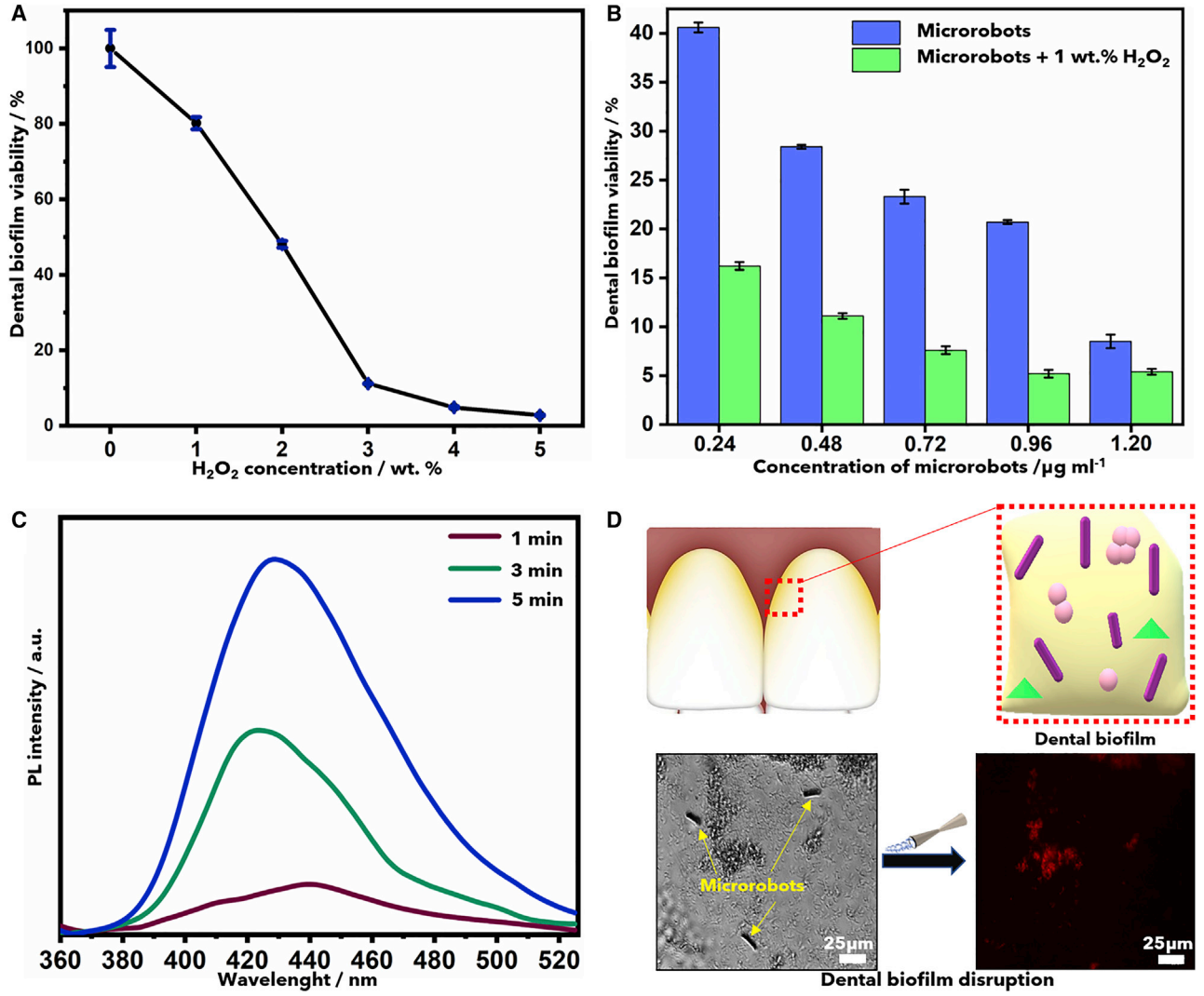

Figure 3. Dental Biofilm Degradation by TiO_2/Pt microrobots

(A) Viability of dental biofilm in the presence of different concentrations of H_2O_2 (n = 8; error bars represent the standard error of the mean).

(B) Viability of dental biofilm after treatment with different concentrations of TiO_2/Pt and their combination with 1 wt% H_2O_2 (n = 4; error bars represent the standard error of the mean).

(C) Fluorescence intensity of 2-hydroxytherepthalic acid resulting from the reaction between terephthalic acid and TiO_2/Pt microrobots in an H_2O_2 solution.

(D) Schematic illustration of dental biofilm degradation by bubble-propelled microrobots and confocal microscopy images showing microrobot-triggered biofilm cell death over time, including a bright-field microscopy image of the biofilm and a fluorescence microscopy image (excitation/emission: 535/617 nm) of the biofilm stained with propidium iodide displaying death cells after 5 min of treatment.

attributed to the following factors: (1) the active motion and continuous generation of O_2 microbubbles by the microrobots, which may significantly contribute to physical disruption of the biofilm or to a biofilm response toward high local O_2 concentrations,[31,46–49] and (2) the simultaneous generation of ROS that have a strong oxidizing power, which promotes cell damage.[25]

The generation of ROS, such as hydroxyl radicals, by the TiO_2/Pt microrobots in the presence of H_2O_2 in the dark was also corroborated by photoluminescence. For this, terephthalic acid was used as a probe molecule, which traps the hydroxyl radicals to produce 2-hydroxyterephthalic acid (fluorescent molecule).[50] As can be seen from Figure 3C, the amount of 2-hydroxyterephthalic acid increased over time,

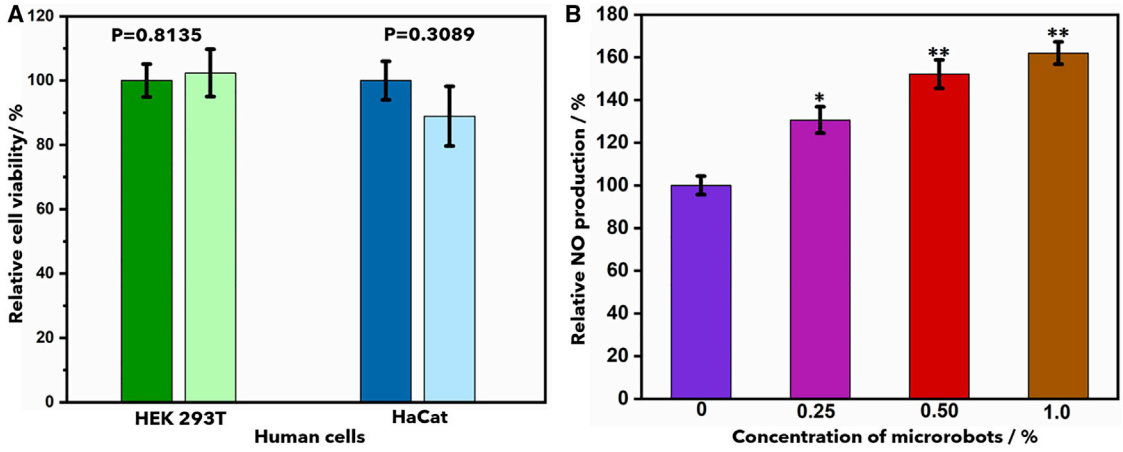

Figure 4. Effect of TiO_2/Pt Microrobots on Human Cells

(A) Cell viability of 2 human cell lines: epithelial cells (HEK293T) and human keratinocytes (HaCaT) in the absence (dark color) and presence (light color) of microrobots (n = 4; error bars represent the standard error of the mean). p values were determined using the Excel t test function (2-tailed distribution, heteroscedastic type).

(B) Relative NO production by macrophages resulting from the immune stimulation induced by the microrobots (n = 4; error bars represent the standard error of the mean). Asterisks indicate the differences between groups and the control (t test, *$p < 0.05$, **$p < 0.005$).

confirming the generation of hydroxyl radicals by the swimming of the TiO_2/Pt microrobots in the peroxide/terephthalic acid solution.[51] Complementarily, the biofilm cell death triggered by the microrobots after 5 min of treatment was also seen using confocal microscope imaging (Figure 3D).

These microrobots could potentially be used for two different approaches: disinfection of orthodontic dental accessories and/or direct dental treatments. In the first case, the microrobots could be recycled by providing them with a magnetic response, *e.g.*, decoration of their structure with magnetic NPs. After treatment of the dental pieces in a solution, the microrobots could be collected by a magnetic bar for further reuse. In the second case, the microrobots could be removed by rinsing the mouth with water several times. Further studies dealing with the development of more cost-effective microrobotic systems for this type of application will be performed in the future.

Considering that the application of the TiO_2/Pt microrobots for dental biofilm disruption would involve the contact of these micromachines with other mouth components, we also investigated the effect of TiO_2/Pt microrobots on the viability of the surface epithelial and epidermis cells. Figure 4A shows the viability of two human cell lines—epithelial cells (HEK293T) and human keratinocyte cells (HaCaT)—in the presence and absence of the microrobots. No toxicity toward the tested human cell lines was found in the presence of microrobots up to the tested concentration.

Since the generation of NO molecules by macrophages is commonly associated with activation of the immune system against bacterial infections,[52] we also evaluated the ability of our microrobots to stimulate NO production. As represented in Figure 4B, an increase in the number of microrobots leads to higher NO production, demonstrating their positive stimulation of the immune system to fight against microbial dental infection.

In conclusion, we have fabricated TiO_2/Pt microrobots with a highly reproducible tubular shape by a membrane template-assisted ALD technique. Due to the

presence of Pt NPs in their inner structure, these microrobots can decompose H_2O_2 into O_2 bubbles. As a proof of concept, we used these TiO_2/Pt microrobots for the degradation of a multispecies-based dental biofilm. It was found that in only 5 min of treatment, these micromachines achieved >95% of biofilm degradation. The killing effect was attributed to the combination of the antibacterial activity of TiO_2/Pt microrobots with the simultaneous generation of hydroxyl radicals and microbubbles on the surface of the biofilm. This work provides an alternative, novel approach based on bubble-propelled microrobots for the potential treatment of dental plaque or decontamination of dental implants. The main advantage includes a synergistic effect of the TiO_2/Pt microrobots with common disinfection agents, such as H_2O_2, that enable the use of lower H_2O_2 concentrations, which is beneficial for repetitive treatments in dentistry applications. Moreover, owing to their autonomous motion and tiny sizes, they could also reach a broader area of the biofilm surface. From an expanded point of view, micromachine-led disruption of biofilms will have a significant impact on a wide scope of biomedical applications.

EXPERIMENTAL PROCEDURES

Resource Availability

Lead Contact

Further information and requests for resources and reagents should be directed to and will be fulfilled by the Lead Contact, Martin Pumera (pumera.research@gmail.com).

Materials Availability

This study did not generate new unique reagents.

Data and Code Availability

The published article and the Supplemental Information include all of the data generated or analyzed during this study.

Materials

Fabrication of TiO_2/Pt Microrobots

TiO_2 tubular microrobots were obtained by ALD by using a PICOSUN R-200 Advanced ALD system. Titanium tetrachloride ($TiCl_4$, 99.99%) and water (Milli-Q) were used as the precursors and N_2 (99.9999% purity) as the carrier gas. A polycarbonate membrane (Whatman, biconical micropores, 2 μm diameter) was used as the template. The deposition parameters were as follows: deposition temperature, 120°C; chamber pressure, 300 Pa; $TiCl_4$ pulse, 0.2 s; N_2 purge, 10 s; H_2O pulse, 1 s; and N_2 purge, 10 s. The pulse sequence was repeated 200 times. Once the TiO_2 tubes were deposited inside the membrane, the membrane was transferred into an H_2PtCl_6 solution (1 mL, 60 mM) containing 3 mL ethanol and polyvinylpyrrolidone (PVP, 20 mg). Then, the Pt NPs were grown inside the tubes by irradiation of the Pt precursor with a UV-vis Osram lamp for 1 h. A change in the color from light yellow to black showed the formation of the Pt NPs. Afterward, the membrane was polished with alumina particles (8 μm) to remove the excess of Pt on the surface. The polished membrane was dissolved in dichloromethane (1 mL) and shaken for 3 min. The released TiO_2/Pt tubes were collected by centrifugation at 9,000 rpm for 5 min. This procedure was repeated 2 more times with dichloromethane. Finally, the microrobots were washed with ethanol and water (3 times each).

Characterization of TiO_2/Pt Microrobots

The morphological and structural characterization of the microrobots was performed by a Tescan MAIA3 microscope equipped with an EDX detector. STEM

images were acquired with a Tescan LYRA dual-beam microscope equipped with a field emission gun (FEG) electron source and STEM sample holder at an electron beam voltage of 30 kV. Attenuated total reflectance (ATR)-FTIR measurements were performed on a NICOLET iS50R FTIR spectrometer (Thermo Scientific). A Diamond ATR crystal and a deuterated triglycine sulfate (DTGS) detector were used for all of the measurements, which were carried out in the range of 4,000−400 cm^{-1} at a resolution of 4 cm^{-1}. The crystal structure of the TiO_2/Pt was determined by XRD using a Bruker D8 Discoverer diffractometer with parafocusing Bragg-Brentano geometry and Cu Kα radiation source. An ethanolic suspension of the microrobots was drop cast several times onto a Si low background sample holder. XRD data were collected in the 2θ range between 20° and 60°.

Motion Characterization of TiO_2/Pt Microrobots

The motion of TiO_2/Pt microrobots was characterized by using an inverted optical microscope (Olympus IX73) equipped with a camera (Retiga R1 CCD). For the recording of the videos, a suspension of the microrobots was placed onto a glass slide, and the fuel solutions were added. The speed and tracking of the microrobots were calculated from the recorded videos using NIS Elements tracking software.

Characterization of the Generation of Hydroxyl Radicals by TiO_2/Pt Microrobots

The generation of hydroxyl radicals by TiO_2/Pt microrobots was examined by the terephthalic acid method. A solution containing H_2O_2 (0.5 wt%), terephthalic acid (0.125 mM), and 25 μL of a suspension of microrobots (100%, 0.0012 mg mL^{-1}) was prepared. The formation of 2-hydroxyterephthalic acid due to the reaction between terephthalic acid and hydroxyl radicals was detected by photoluminescence (PL) using a Fluorolog Extreme (Horiba) system equipped with a Xe lamp (450 W), a double-excitation monochromator, and an iHR320 monochromator with a thermoelectrically cooled photomultiplier tube (PMT) detector. The PL spectrum was obtained from 360 to 550 nm at a 312-nm excitation wavelength.

Cytotoxicity of TiO_2/Pt Microrobots

The toxicity of the mammalian tissue culture was studied on HEK293T ATCC CRL-11268TM (epithelial cells) and HaCaT CLS 300493 (human keratinocyte). The cells were cultured in standard Dulbecco's modified Eagle's medium (DMEM) supplemented with fetal bovine serum (FBS, 10%) and 1× antibiotic antimycotic solution and subcultured 2×/week by a standardized detachment procedure using trypsin-EDTA (0.25%). After 72 h of the toxicity experiment, the cells were harvested from exponential-phase cultures and the cell number was counted automatically using Cellometer Auto T4 Automated Cell Counter (Nexcelom Bioscience). For the cytotoxicity experiments, 100 μL 1 × 10^5 cells mL^{-1} were seeded into each well of a 96-well plate. The microrobots (0.0012 mg mL^{-1}) were tested in triplicate within the same experiment. The cell viability was evaluated after 72 h of incubation by the standard resazurin assay.[53]

Immunomodulatory Effect of TiO_2/Pt Microrobots

The murine macrophage RAW 264.7 cell line was used to determine the effect of the microrobots on macrophages. The cells were cultured according to the standardized procedure as described above. For the experiment, 100 μL 1 × 10^6 cells mL^{-1} were seeded into each well of a 96-well plate. After 48 h, the DMEM medium was changed for essential medium Eagle no phenol red (MEM), the cells were washed 3× with phosphate-buffered saline (PBS), and *E. coli* lipopolysaccharide (LPS, 1 μg mL^{-1} in MEM) and different concentration of micromotors (1 μL) were added to a final volume of 100 μL. After 24 h, the medium was mixed with Griess reagent (0.04 g mL^{-1}, prepared

fresh in deionized water) in a 1:1 ratio in a new 96-well plate. The absorbance was measured at 540 nm after 15 min. The cell viability was evaluated after 72 h of incubation by standard resazurin assay. All of the experiments were performed in triplicate.

Since NO is highly unstable, it undergoes oxidative degradation into nitrite and nitrate ions. Thus, the Griess method consists of the indirect determination of NO by the measurement of those stable compounds by UV-vis spectrophotometry.[54] The Griess reaction involves the reaction of the nitrite ion with sulfanilamide, forming a diazonium salt as a product. The resulting product reacts with *N*-1-naphthyl ethylenediamine dihydrochloride to form an azo product with a pink-red color, which is measured at 540 nm.

Dental Biofilm Disruption Experiments

The ability of the TiO_2/Pt microrobots to disrupt a biofilm was tested in a multispecies dental biofilm consisting of *S. gordonii* (DSM 6777), *V. parvula* (DSM 2008), *F. nucleatum subsp. nucleatum* (DSM 15643), and *A. naeslundii* (DSM 43013). The assays were performed in 96-well plates. The overnight culture of each strain was diluted with brain heart infusion (BHI) broth to obtain turbidity equal to a 0.5 McFarland standard. After that, the mixed bacterial suspension was prepared in a volume ratio of 1:1:1:1 and aliquots (100 μL) were pipetted into each well of the plate. After 72 h of incubation at 37°C, the medium was removed, and the wells were washed 3× with PBS (pH 7.4). The non-toxic concentration of H_2O_2 was determined by adding different concentrations of H_2O_2 (from 0 to 5 wt%) in sterile deionized water into each well. The experiment was realized in a total volume of 100 μL and each test was repeated 8×. The highest concentration of H_2O_2 with percentages of cell viability >80% was considered non-cytotoxic according to ISO 10993-5. The toxicity of microrobots was determined by the application of different concentrations of microrobots (from 0.24 to 1.2 μg mL^{-1}) in sterile deionized water into each well. The experiment was realized in a total volume of 100 μL and each test was repeated 4×. The disruption of biofilms by moving microrobots was realized by the addition of different concentrations of microrobots in sterile deionized water supplemented with the non-toxic concentration of H_2O_2 (1 wt%) into each well. The experiment was realized in a total volume of 100 μL and each test was repeated 4×. After 5 min of incubation with each control, the solution was removed, the wells were washed 3× by PBS, and resazurin in PBS (100 μL, 0.03 mg mL^{-1}) was added.[53] The viability of the biofilm was evaluated by measuring the fluorescence (560/590 nm, excitation/emission) of the samples.

The biofilm was visualized by using an Andor Revolution XD (Andor Technology) confocal microscope. The biofilm was washed 3× with PBS (pH 7.4). Then, the staining solution containing propidium iodide (PI, 39 μg mL^{-1}) in water was applied for 5 min. Finally, the staining solution was removed, and the biofilm was washed 3× with PBS (pH 7.4). The excitation and emission wavelengths were 535 and 617 nm, respectively. The figures were edited using ImageJ 1.51 s software (National Institutes of Health).

Data Processing and Statistical Analysis

The experiments were done in (n) repetitions, as stated in each figure. The data are presented as the averages of the repetitions with the standard error of the mean (SEM). Statistical significance was verified with the Excel t test function (two-tailed distribution, heteroscedastic type). One-way analysis of variance (ANOVA) was used followed by Duncan's post hoc test ($p < 0.05$) to show the differences between the groups. For ANOVA, Statistica software version 12 (Tibco Software) was used.

SUPPLEMENTAL INFORMATION

Supplemental Information can be found online at https://doi.org/10.1016/j.xcrp.2020.100181.

ACKNOWLEDGMENTS

M.P. was supported by Ministry of Education, Youth, and Sports grant LL2002 under ERC CZ program.

AUTHOR CONTRIBUTIONS

Conceptualization, K.V., T.R., and M.P.; Methodology, K.V., T.R., and M.P.; Investigation, K.V. (synthesis and characterization of the microrobots), J.V. and L.H. (biological experiments), and J.P. (TiO_2-ALD deposition); Writing – Original Draft, K.V. and J.V.; Writing – Review & Editing, K.V., J.P., T.R., J.V., and M.P.; Funding Acquisition, M.P.; Resources, M.P. and T.R.; Supervision, M.P.

DECLARATION OF INTERESTS

The authors declare no competing interests.

Received: May 5, 2020
Revised: July 2, 2020
Accepted: August 4, 2020
Published: September 9, 2020

REFERENCES

1. Parmar, J., Vilela, D., Villa, K., Wang, J., and Sánchez, S. (2018). Micro- and Nanomotors as Active Environmental Microcleaners and Sensors. J. Am. Chem. Soc. *140*, 9317–9331.
2. Abdelmohsen, L.K.E.A., Peng, F., Tu, Y., and Wilson, D.A. (2014). Micro- and nano-motors for biomedical applications. J. Mater. Chem. B Mater. Biol. Med. *2*, 2395–2408.
3. Luo, M., Feng, Y., Wang, T., and Guan, J. (2018). Micro-/Nanorobots at Work in Active Drug Delivery. Adv. Funct. Mater. *28*, 1706100.
4. Villa, K., Krejčová, L., Novotný, F., Heger, Z., Sofer, Z., and Pumera, M. (2018). Cooperative Multifunctional Self-Propelled Paramagnetic Microrobots with Chemical Handles for Cell Manipulation and Drug Delivery. Adv. Funct. Mater. *28*, 1804343.
5. Palacci, J., Sacanna, S., Vatchinsky, A., Chaikin, P.M., and Pine, D.J. (2013). Photoactivated colloidal dockers for cargo transportation. J. Am. Chem. Soc. *135*, 15978–15981.
6. Villa, K., Novotný, F., Zelenka, J., Browne, M.P., Ruml, T., and Pumera, M. (2019). Visible-Light-Driven Single-Component $BiVO_4$ Micromotors with the Autonomous Ability for Capturing Microorganisms. ACS Nano *13*, 8135–8145.
7. Jurado-Sánchez, B., and Escarpa, A. (2017). Janus Micromotors for Electrochemical Sensing and Biosensing Applications: A Review. Electroanalysis *29*, 14–23.
8. Campuzano, S., Esteban-Fernández de Ávila, B., Yáñez-Sedeño, P., Pingarrón, J.M., and Wang, J. (2017). Nano/microvehicles for efficient delivery and (bio)sensing at the cellular level. Chem. Sci. (Camb.) *8*, 6750–6763.
9. Villa, K., and Pumera, M. (2019). Fuel-free light-driven micro/nanomachines: artificial active matter mimicking nature. Chem. Soc. Rev. *48*, 4966–4978.
10. Pourrahimi, A.M., Villa, K., Ying, Y., Sofer, Z., and Pumera, M. (2018). ZnO/ZnO_2/Pt Janus Micromotors Propulsion Mode Changes with Size and Interface Structure: Enhanced Nitroaromatic Explosives Degradation under Visible Light. ACS Appl. Mater. Interfaces *10*, 42688–42697.
11. Villa, K., Manzanares Palenzuela, C.L., Sofer, Z., Matějková, S., and Pumera, M. (2018). Metal-Free Visible-Light Photoactivated C_3N_4 Bubble-Propelled Tubular Micromotors with Inherent Fluorescence and On/Off Capabilities. ACS Nano *12*, 12482–12491.
12. Katuri, J., Ma, X., Stanton, M.M., and Sánchez, S. (2017). Designing Micro- and Nanoswimmers for Specific Applications. Acc. Chem. Res. *50*, 2–11.
13. Larsen, T., and Fiehn, N.-E. (2017). Dental biofilm infections - an update. APMIS *125*, 376–384.
14. Flemming, H.-C., Wingender, J., Szewzyk, U., Steinberg, P., Rice, S.A., and Kjelleberg, S. (2016). Biofilms: an emergent form of bacterial life. Nat. Rev. Microbiol. *14*, 563–575.
15. Costerton, J.W., Cheng, K.J., Geesey, G.G., Ladd, T.I., Nickel, J.C., Dasgupta, M., and Marrie, T.J. (1987). Bacterial biofilms in nature and disease. Annu. Rev. Microbiol. *41*, 435–464.
16. Schmidt, J.C., Zaugg, C., Weiger, R., and Walter, C. (2013). Brushing without brushing?–a review of the efficacy of powered toothbrushes in noncontact biofilm removal. Clin. Oral Investig. *17*, 687–709.
17. Chi, Q., Wang, Z., Tian, F., You, J., and Xu, S. (2018). A Review of Fast Bubble-Driven Micromotors Powered by Biocompatible Fuel: Low-Concentration Fuel, Bioactive Fluid and Enzyme. Micromachines (Basel) *9*, 537.
18. Mou, F., Li, Y., Chen, C., Li, W., Yin, Y., Ma, H., and Guan, J. (2015). Single-Component TiO_2 Tubular Microengines with Motion Controlled by Light-Induced Bubbles. Small *11*, 2564–2570.
19. Giudicatti, S., Marz, S.M., Soler, L., Madani, A., Jorgensen, M.R., Sanchez, S., and Schmidt, O.G. (2014). Photoactive rolled-up TiO_2 microtubes: fabrication, characterization and applications. J. Mater. Chem. C Mater. *2*, 5892–5901.
20. Li, J., Liu, W., Wang, J., Rozen, I., He, S., Chen, C., Kim, H.G., Lee, H.-J., Lee, H.-B., Kwon, S.-H., et al. (2017). Nanoconfined Atomic Layer Deposition of TiO_2/Pt Nanotubes: Toward Ultrasmall Highly Efficient Catalytic Nanorockets. Adv. Funct. Mater. *27*, 1700598.
21. Liu, L., Bai, T., Chi, Q., Wang, Z., Xu, S., Liu, Q., and Wang, Q. (2017). How to Make a Fast, Efficient Bubble-Driven Micromotor: A Mechanical View. Micromachines (Basel) *8*, 267.
22. Ramos, K.B., Clavel, G., Marichy, C., Cabrera, W., Pinna, N., and Chabal, Y.J. (2013). In Situ Infrared Spectroscopic Study of Atomic Layer-Deposited TiO_2 Thin Films by Nonaqueous Routes. Chem. Mater. *25*, 1706.
23. Zhang, H., Wang, X., Li, N., Xia, J., Meng, Q., Ding, J., and Lu, J. (2018). Synthesis and

Characterization of TiO_2/Graphene Oxide Nanocomposites for Photoreduction of Heavy Metal Ions in Reverse Osmosis Concentrate. RSC Advances *8*, 34241–34251.

24. Hayakawa, M., Onoe, H., Nagai, K.H., and Takinoue, M. (2016). Influence of Asymmetry and Driving Forces on the Propulsion of Bubble-Propelled Catalytic Micromotors. Micromachines (Basel) *7*, 229.

25. Tredwin, C.J., Naik, S., Lewis, N.J., and Scully, C. (2006). Hydrogen peroxide tooth-whitening (bleaching) products: review of adverse effects and safety issues. Br. Dent. J. *200*, 371–376.

26. Walsh, L.J. (2000). Safety issues relating to the use of hydrogen peroxide in dentistry. Aust. Dent. J. *45*, 257–269, 289.

27. Liang, C., Zhan, C., Zeng, F., Xu, D., Wang, Y., Zhao, W., Zhang, J., Guo, J., Feng, H., and Ma, X. (2018). Bilayer Tubular Micromotors for Simultaneous Environmental Monitoring and Remediation. ACS Appl. Mater. Interfaces *10*, 35099–35107.

28. Dong, R., Wang, C., Wang, Q., Pei, A., She, X., Zhang, Y., and Cai, Y. (2017). ZnO-based microrockets with light-enhanced propulsion. Nanoscale *9*, 15027–15032.

29. Liu, W., Ge, H., Gu, Z., Lu, X., Li, J., and Wang, J. (2018). Electrochemical Deposition Tailors the Catalytic Performance of MnO_2 -Based Micromotors. Small *14*, e1802771.

30. Beladi-Mousavi, S.M., Klein, J., Khezri, B., Walder, L., and Pumera, M. (2020). Active Anion Delivery by Self-Propelled Microswimmers. ACS Nano *14*, 3434–3441.

31. Stanton, M.M., Park, B.-W., Vilela, D., Bente, K., Faivre, D., Sitti, M., and Sánchez, S. (2017). Magnetotactic Bacteria Powered Biohybrids Target E. coli Biofilms. ACS Nano *11*, 9968–9978.

32. Hwang, G., Paula, A.J., Hunter, E.E., Liu, Y., Babeer, A., Karabucak, B., Stebe, K., Kumar, V., Steager, E., and Koo, H. (2019). Catalytic Antimicrobial Robots for Biofilm Eradication. Sci. Robot. *4*, eaaw2388.

33. Gao, L., Liu, Y., Kim, D., Li, Y., Hwang, G., Naha, P.C., Cormode, D.P., and Koo, H. (2016). Nanocatalysts promote Streptococcus mutans biofilm matrix degradation and enhance bacterial killing to suppress dental caries in vivo. Biomaterials *101*, 272–284.

34. Jones, C.G. (1997). Chlorhexidine: is it still the gold standard? Periodontol. 2000 *15*, 55–62.

35. Cervone, F., Tronstad, L., and Hammond, B. (1990). Antimicrobial effect of chlorhexidine in a controlled release delivery system. Endod. Dent. Traumatol. *6*, 33–36.

36. US Department of Health and Human Services, Food and Drug Administration (2016). Use of International Standard ISO 10993-1, "Biological evaluation of medical devices—Part 1: Evaluation and testing within a risk management process." Guidance for Industry and Food and Drug Administration Staff. https://fda.gov/media/85865/download.

37. Ahmadi-Motamayel, F., Falsafi, P., Goodarzi, M.T., and Poorolajal, J. (2017). Evaluation of salivary catalase, vitamin C, and alpha-amylase in smokers and non-smokers: a retrospective cohort study. J. Oral Pathol. Med. *46*, 377–380.

38. Van den Driessche, F., Rigole, P., Brackman, G., and Coenye, T. (2014). Optimization of resazurin-based viability staining for quantification of microbial biofilms. J. Microbiol. Methods *98*, 31–34.

39. Sánchez, L.D., Taxt-Lamolle, S.F.M., Hole, E.O., Krivokapić, A., Sagstuen, E., and Haugen, H.J. (2013). TiO_2 Suspension Exposed to H_2O_2 in Ambient Light or Darkness: Degradation of Methylene Blue and EPR Evidence for Radical Oxygen Species. Appl. Catal. B *142–143*, 662–667.

40. Rincón, A.-G., and Pulgarin, C. (2006). Comparative Evaluation of Fe^{3+} and TiO_2 Photoassisted Processes in Solar Photocatalytic Disinfection of Water. Appl. Catal. B *63*, 222–231.

41. Ogino, C., Dadjour, M.F., Iida, Y., and Shimizu, N. (2008). Decolorization of methylene blue in aqueous suspensions of titanium peroxide. J. Hazard. Mater. *153*, 551–556.

42. Adams, L.K., Lyon, D.Y., and Alvarez, P.J.J. (2006). Comparative eco-toxicity of nanoscale TiO_2, SiO_2, and ZnO water suspensions. Water Res. *40*, 3527–3532.

43. Vargas, M.A., and Rodríguez-Páez, J.E. (2019). Facile Synthesis of TiO_2 Nanoparticles of Different Crystalline Phases and Evaluation of Their Antibacterial Effect Under Dark Conditions Against E. Coli. J. Clust. Sci. *30*, 379–391.

44. Fenoglio, I., Greco, G., Livraghi, S., and Fubini, B. (2009). Non-UV-induced radical reactions at the surface of TiO_2 nanoparticles that may trigger toxic responses. Chemistry *15*, 4614–4621.

45. Randorn, C., Wongnawa, S., and Boonsin, P. (2004). Bleaching of Methylene Blue by Hydrated Titanium Dioxide. Sci. Asia *30*, 149.

46. Seo, Y., Leong, J., Park, J.D., Hong, Y.-T., Chu, S.-H., Park, C., Kim, D.H., Deng, Y.-H., Dushnov, V., Soh, J., et al. (2018). Diatom Microbubbler for Active Biofilm Removal in Confined Spaces. ACS Appl. Mater. Interfaces *10*, 35685–35692.

47. Wiedmer, D., Petersen, F.C., Lönn-Stensrud, J., and Tiainen, H. (2017). Antibacterial effect of hydrogen peroxide-titanium dioxide suspensions in the decontamination of rough titanium surfaces. Biofouling *33*, 451–459.

48. Parini, M.R., Eggett, D.L., and Pitt, W.G. (2005). Removal of Streptococcus mutans biofilm by bubbles. J. Clin. Periodontol. *32*, 1151–1156.

49. Yamada, J., Takiguchi, T., Saito, A., Odanaka, H., Soyama, H., and Yamamoto, M. (2017). Removal of Oral Biofilm on an Implant Fixture by a Cavitating Jet. Implant Dent. *26*, 904–910.

50. Hirakawa, T., Yawata, K., and Nosaka, Y. (2007). Photocatalytic Reactivity for O2− and OH Radical Formation in Anatase and Rutile TiO2 Suspension as the Effect of H2O2 Addition. Appl. Catal. A *325*, 105–111.

51. Parmar, J., Villa, K., Vilela, D., and Sánchez, S. (2017). Platinum-Free Cobalt Ferrite Based Micromotors for Antibiotic Removal. Appl. Mater. Today *9*, 605–611.

52. Fang, F.C., and Vazquez-Torres, A. (2002). Nitric oxide production by human macrophages: there's NO doubt about it. Am. J. Physiol. Lung Cell. Mol. Physiol. *282*, L941–L943.

53. Sittampalam, G.S., Grossman, A., Brimacombe, K., Arkin, M., Auld, D., Austin, C.P., Baell, J., Bejcek, B., Caaveiro, J.M.M., Chung, T.D.Y., et al. (2004). The Assay Guidance Manual (Eli Lilly & Company and the National Center for Advancing Translational Sciences).

54. Bryan, N.S., and Grisham, M.B. (2007). Methods to detect nitric oxide and its metabolites in biological samples. Free Radic. Biol. Med. *43*, 645–657.